HIGHLY RELIABLE AERODYNAMIC CALIBRATION FOR GROUND AND FLIGHT TESTING TOTAL TEMPERATURE PROBES

F. Fontaneto
"Jacques Chauvin" Laboratory
von Karman Institute for Fluid Dynamics
Rhode-St-Genèse – Belgium

e-mail: fontaneto@vki.ac.be

A. Lahalle
"Jacques Chauvin" Laboratory
von Karman Institute for Fluid Dynamics
Rhode-St-Genèse – Belgium

e-mail: lahalle@vki.ac.be

ABSTRACT

All along the development of a new aero-engine, testing is constantly performed. It provides validation data during the design stage but it also assures the manufactures of the fulfillment of the certification requirements. The equipment used in the testing phase and the quality of the performed measurements have therefore a crucial importance which directly justifies the attention given to the instrumentation calibration.

The present paper describes, in sort of step-by-step evolution, the development of a highly reliable aerodynamic calibration procedure for high performance total temperature probes.

NOMENCLATURE

η	Recovery factor
P	Pressure
T	Temperature
Ma	Mach number

Subscripts

0	total quantity
n	referred to nozzle
p	referred to probe

INTRODUCTION

Ground and flying testing provide crucial information along the whole development phase of an aero-engine. On one hand, experimental data are required to validate numerical simulations, currently the main design tool used by manufacturers. On the other hand, internal testing provides confidence for the achievement of the certification milestone, after which the product can finally be commercialized.

Typical instrumentation normally employed for this purpose, are total temperature / total pressure probes. Figure 1 shows an example of such item as designed at the von Karman Institute for Fluid Dynamics (VKI). It consists of a body (A) which allows for a precise and safe mounting in the machine and which is also equipped with a reference index for alignment purposes. The stem (B) structurally supports the measuring heads (C) and provides the path for wirings and pneumatic connections. The measuring heads (a detailed view is reported in Figure 2) are of Kiel type with two ventilation holes on the lateral sides. The oval shape of the measuring head allows hosting a pressure and a temperature sensor at the same time.
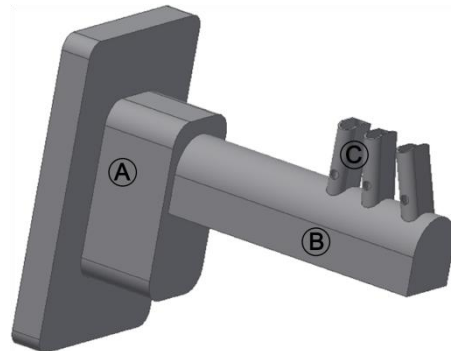

Figure 1: in-house designed total temperature / total pressure probe. (A) probe body; (B) probe stem; (C) measuring heads. Adapted from Lahalle [1].

Pressure and Temperature sensors

Ventilation hole

Figure 2: detailed view of the measuring heads. Adapted from Lahalle [1].

The calibration of this type of instrumentation normally coincides with the evaluation of the so called recovery factor (η). The latter quantifies how efficiently a probe recovers the total quantity of interest (X) and it is normally defined as the ratio between the measured value and the real one (Equation 1). η can be measured as a function of Mach and Reynolds numbers while, by systematically varying the flow angles, the insensibility range of the Kiel heads can also be retrieved.

$$\eta = \frac{X_{measured}}{X_{real}} \le 1 \qquad (1)$$

In light of what was discussed in the first paragraph, a high quality calibration is a mandatory prerequisite when flying and ground testing instrumentation are considered. Generally speaking, three main requirements must be taken into account:

- The calibration process should be free from uncontrolled experimental errors.
- The calibration uncertainty should be precisely quantified.
- The calibration uncertainty should be as small as possible.

The present paper describes, in sort of a step-by-step evolution, the development at the von Karman Institute of a highly reliable calibration procedure for high performance total temperature probes which fully complies with the aforementioned requirements. The committed early errors and the faced issues are described in detail while the actions taken for their solution are presented and critically commented. In the end, a complete description of the experimental setup and of the measurement chain is provided together with a detailed overview on the uncertainty computation methodology.
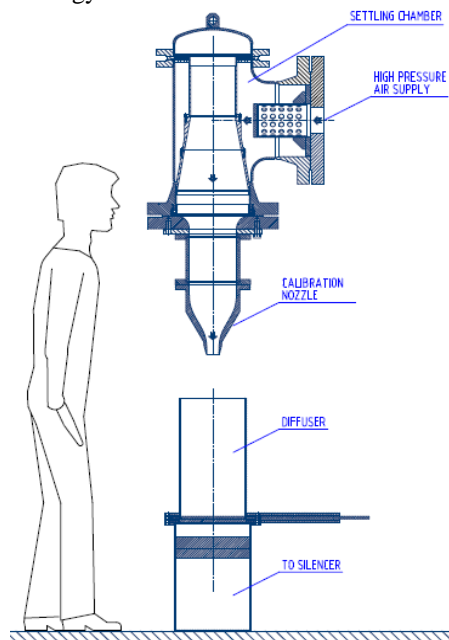

Figure 3: the C4 high speed calibration nozzle of VKI.

THE C4 CALIBRATION FACILITY

The C4 high speed calibration facility of VKI (Figure 3) consists of a convergent nozzle of 50 [mm] in exit diameter, discharging at atmospheric conditions. The nozzle is supplied by a settling chamber equipped with several mesh screens to reduce flow swirling and turbulence. Thanks to the high contraction ratio (D_{in}/D_{exit} = 14.75), the Mach number at the nozzle inlet is as high as 0.05 for

chocked exit conditions. The nozzle total inlet pressure and temperature are measured at the inlet of nozzles by means of six different T_0 and P_0 measurement points, allowing to verify the homogeneity of the inlet flow field and to retrieve circumferentially averaged values.

The facility is supplied by the 40 [bar] pressure line of the institute and it is operated in a blow-down mode. A 2-stages piston compressor fills two reservoir of 70 [m³] of total capacity which are then discharged during the test. Such configuration leads to limited testing times and to important total temperature variation during the test.

FIRST CALIBRATION SETUP

Figure 4 shows the very first calibration setup adopted for total temperature probes calibrations. The probe's thermocouple and 4 temperature ports in the nozzle were acquired by means of a Scanivalve DTS-4050 temperature scanner. The two remaining nozzle's temperature ports were equipped with calibrated resistance thermometers (PT100) which were used for verification purposes and acquired by a precision 4-wire Ohmmeter.
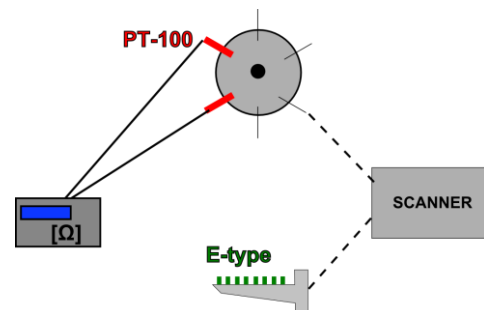

Figure 4: first experimental setup for total temperature probes calibration.

The result of a first calibration attempt is presented in Figure 5 for four different probes. Even though probe 1 exhibits an unphysical flat evolution with the Mach number, the measured η_T values keep below unity while the three remaining probes all provide values higher than 1.
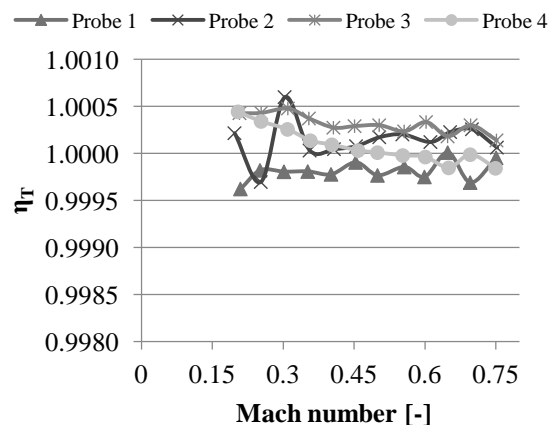

Figure 5: results of the first calibration attempt for 4 different total temperature probes.

The substancial incoherency of the latter results can be explained by means of the analysis reported in Equations 2. If the nozzle total temperature and the probe recovery factor set equal to 288 [K] and 0.999 respectively, then the corresponding temperature difference $\Delta T = T_{0,nozzle} - T_{0,probe}$ would be of the order of 0.3 degrees, exactly the same magnitude as the uncertainty of the temperature scanner (±0.25 degrees).

$$T_{0,nozzle} = 288 \ [K]$$
$$\eta_T = 0.999 = \frac{T_{0,probe}}{T_{0,nozzle}} = \frac{T_{0,nozzle} - \Delta T}{T_{0,nozzle}} \qquad (2)$$
$$\Delta T = T_{0,nozzle} - T_{0,probe} = 0.29 \ [°]$$
$$\delta T_{scanner} = \pm 0.25 \ [°]$$

LAWS OF THERMOELECTRICITY

The direct conclusion of the previous analysis was therefore that the accuracy of the complete measurement chain had to be improved and, at such extent, the laws of thermoelectricity were considered.

Figure 6 provides a graphical representation of the thermocouple effect (the Seebeck effect). By joining together two materials of different thermoelectric polarity (different slopes on Figure 6b), a net voltage is generated when the two junctions are kept at different temperatures.
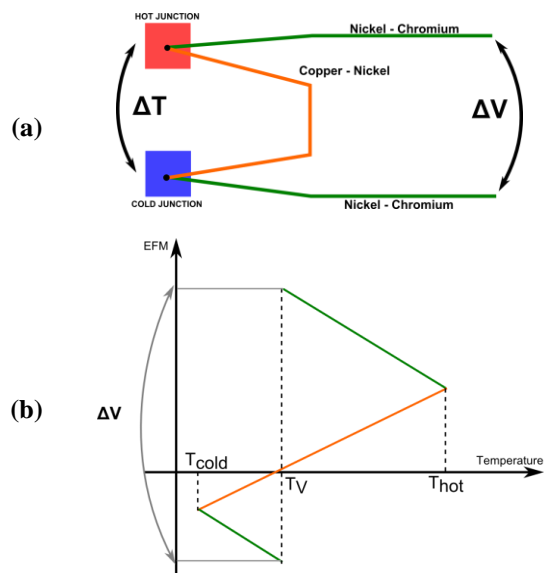

Figure 6: Seebeck effect for an E-type thermocouple. (a) scheme of connections; (b) EFM vs. temperature evolution.

Standard electronics for thermocouple measurements simulate the presence of the second junction by means of a stabilized electronic circuit. The so generated ΔT is then measured and transformed in absolute terms by summing it to the measurement of an absolute reference thermometer normally embedded in the electronic itself. This step corresponds to the main loss of accuracy in the measurement chain as two uncertainties are linearly

summed together but it also suggests that a substantial improvement can be achieved if the ΔT could be directly measured with precision.

The latter configuration clearly implies the adoption of two thermocouples whose homogeneity is a crucial requirement. Typical thermocouple inhomogeneities are metallic inclusions, plastic deformations and changes in chemical composition (e.g. oxidization). The presence of inhomogeneities directly translates into a variation of the thermoelectric polarity of materials which leads to the generation of spurious voltage differentials. When adopting therefore such configuration a homogeneity check is a mandatory and simple operation: as shown by Figure 7, by simply submitting the two junctions to the same temperature, one can verify if the open-end voltage is equal or different from zero.
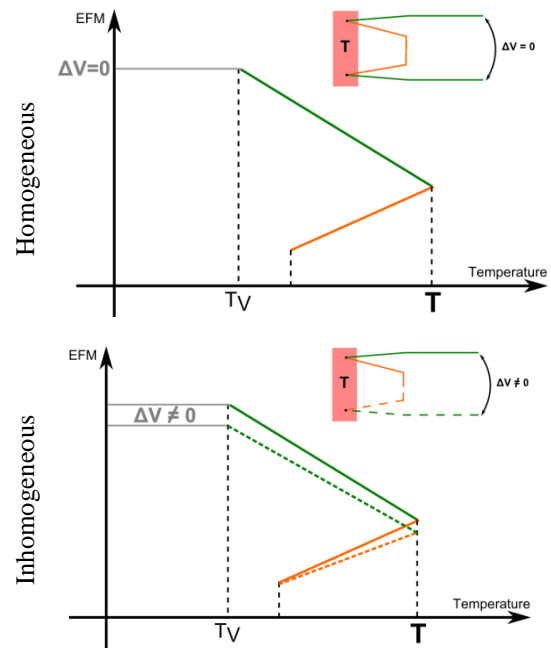

Figure 7: effects of material inhomogeneities on the 2-junction thermocouple configuration.

If the homogeneity of materials cannot be assured, the adoption of a 3-junction configuration can also be considered. As visible from Figure 8a, two junctions can be created by welding a third material (e.g. a copper wire) to the leads of a single thermocouple. Submitting therefore the latters to the same temperature, a ΔV can be measured which is proportional to the temperature difference between hot and cold sources (Figure 8b). This solution benefits from being intrinsically free from homogeneity issues (except from those related to the third material) but spurious results can still be retrieved if the two reference junctions are not kept exactly at the same temperature.

In order to determine which configuration provides the most robust experimental setup, a sensitivity analysis was performed for an E-type

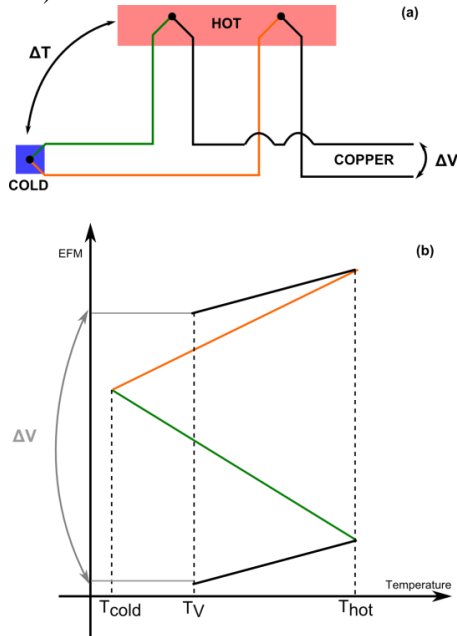thermocouple operated in typical C4 conditions (Table 1).

Figure 8: 3-junction configuration for referenced thermocouple measurements.

T [K]	288	*Cold junction temperature*
T_V [K]	293	*Voltmeter leads temperature*
$m_{E\text{-type}}$ [$\mu V/°$]	58.7	*E-type coefficient*

Table 1: numerical values used for the sensitivity analysis.

2-junction configuration

By expressing the mathematical equations leading to Figure 6b, one can demonstrate that the sensitivity of ΔV with respect to $m_{E\text{-type}}$ only depends on $T-T_V$ (Equation 3a). Assuming that the uncertainty related to the E-type coefficient equals the 5% of its value, the induced error on ΔV results to be in the order of 15 [μV] (Equation 3b).

$$\frac{\partial \Delta V}{\partial m_{E-type}} = T - T_V \tag{3a}$$

$$\delta \Delta V = \frac{\partial \Delta V}{\partial m_{E-type}} \cdot \delta m_{E-type} = 14.7 \ [\mu V] \tag{3b}$$

3-junction configuration

Differentiating the expression of ΔV for Figure 8b with respect to the hot junctions temperature difference ($\Delta T_{H,junction}$), it can be shown that such sensitivity only depends on the algebraic sum of the thermoelectric polarities of each material (Equation 4a). Taking $\Delta T_{H,junction} = 0.5$ [°], a total error on the voltage differential of 8.25 [μV] (Equation 4b) is retrieved.

$$\frac{\partial \Delta V}{\partial \Delta T_{H,junction}} = m_{copper} - m_{metal1} - m_{metal2} \tag{4a}$$

$$\delta \Delta V = \frac{\partial \Delta V}{\partial \Delta T_{H,junction}} \cdot \Delta T_{H,junction} = 8.25 \ [\mu V] \tag{4b}$$

The assumed values for $\delta m_{E\text{-type}}$ and $\delta \Delta T_{H,junction}$ are extremely conservative but they highlight that the 3-junction solution normally provides the best results in terms of accuracy. Nevertheless, it has also to be considered that this configuration normally requires a bigger access space to the facility while, on the other hand, a calibration can be always performed in the case of the 2-junction solution if homogeneity issues arise.

Basing therefore on the previous analysis and on the latter considerations, a 2-junction configuration was adopted in the experimental setup.

2-JUNCTION CALIBRATION SETUP

Figure 9 shows the evolution of the experimental setup taking into account the previously discussed conclusions. The probe's thermocouple was referenced to a thermocouple positioned in the nozzle. Care was taken in using two thermocouples of the same batch which were previously verified for materials homogeneity. The temperature difference between the nozzle and the probe was acquired by means of a precision nano-voltmeter. The remaining parts of the setup were kept as in the original configuration.
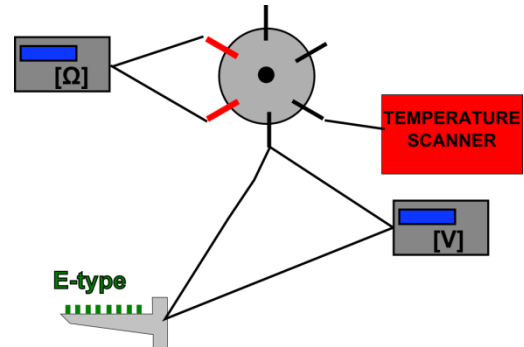

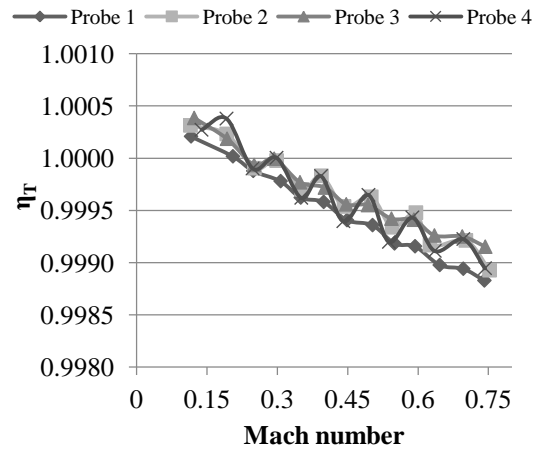**Figure 9: 2-junction calibration setup layout.**

Figure 10: calibration results for 4 different total temperature probes obtained by implementing the 2-junction thermocouple configuration.

The adoption of a 2-junctions thermocouple configuration allowed retrieving a physical evolution of the calibration data: a negative slope with the Mach number is clearly visible in Figure 10 while, at the same time, the scatter between the calibration curves of the different probes is strongly reduced. On the other hand, data still exhibit values higher than unity at low velocity and a marked wavy behavior can be observed.

Since during the blow-down the total inlet temperature drops of several degrees, a pre-cooling phase was mandatory to stabilize the recovery factor before the beginning of the calibration. This effect is shown in Figure 11 which reports the nozzle total temperature time series for a stable operative condition of the facility (Ma=0.65), plotted against the evolution in time of the recovery factor. At the beginning of the pre-cooling phase, the nozzle temperature reduces while η_T rises to values higher than unity. When $T_{0,nozzle}$ reaches its minimum, the recovery factor starts decreasing, with an asymptotic trend towards a stable and physical value which keeps constant despite an increasing of the nozzle temperature.
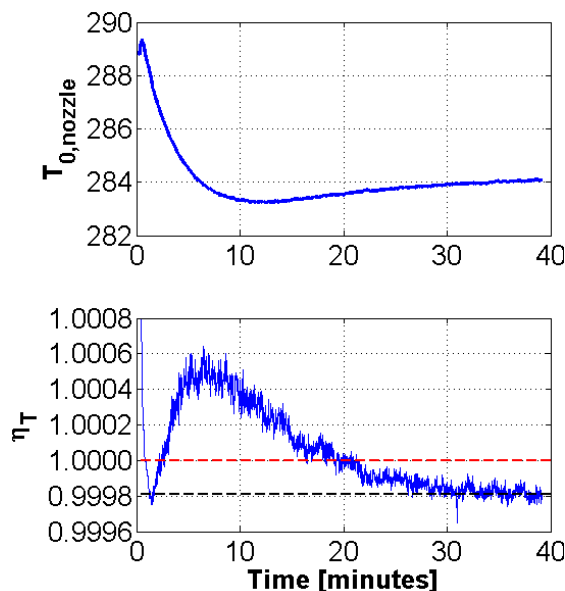

Figure 11: nozzle temperature transient during blow-down, plotted against the recovery factor evolution in time.

In the first part, conduction clearly dominates the results. The thermal inertia of the probe is such that the probe keeps warmer than the incoming flow, leading therefore to unphysical recovery factor values. Successively, when the nozzle's temperature rises again, the temperature difference that drives the conduction error reduces, slowly heading towards the last part of the time series where thermal equilibrium is reached.

A typical test procedure implied to perform the pre-cooling phase at the highest tested Mach number within the calibration. Once the recovery factor was stabilized for at least 5 minutes, the Mach number was varied systematically to each operative condition foresaw by the test matrix. In particular, for repeatability purposes, half of the calibration points were taken in a descending fashion, from the highest to the lowest condition, while the remaining points were swept by increasing systematically the Mach number, filling the gaps (see Figure 12).

In light of what has been just discussed, it is straightforward to address both the too high recovery factors at low speed and the wavy evolution of the calibration curve to the presence of an important conduction effect persisting also after the end of the pre-cooling phase. At low Mach numbers, the cooling power of the main stream was too low to efficiently counter-balance the conduction through the probe. Indeed, its body was covered by the nozzle's stream only for a small part while the biggest portion of the stem was kept at ambient conditions. As a result, the probe was warming up, leading to η_T values higher than unity and to the generation of the wavy calibration evolution.
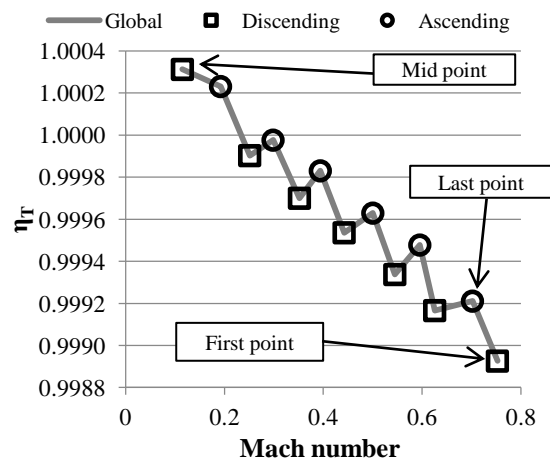

Figure 12: calibration procedure after the pre-cooling phase.

The direct conclusion from the previous results is that a reliable total temperature probe calibration can only be carried out if adiabatic conditions are generated between the nozzle total temperature and the room temperature. At the same time, as evident from Figure 11, the pre-cooling phase was accounting for a substantial item in the whole calibration cost as a result of the extremely long waiting time (about 40 minutes) and of the very high discharged massflows (0.64 [kg/s] when blowing at Ma = 0.75).

FINAL CALIBRATION SETUP

In order to overcome the issues encountered within the previous setup, a modification to the facility was required. A PID-controlled 36 [kW] Sylvania in-line heater was mounted before the plenum feeding point while the feedback

thermocouple was instead directly placed in the nozzle, at the same exact position of the total inlet temperature measurement points.

Figure 13 reports the calibration curves for the central head of the probe shown in Figure 1 which was calibrated after the implementation of the final setup. The evolution of the recovery factor with the Mach number preserves the classical negative slope already achieved by the adoption of the 2-junction measurement configuration while providing a much more limited scatter of results and no over-shoot above 1 at low Mach numbers. The same conclusions can be drawn for the pressure recovery factor that also exhibits a typical descending evolution with Mach.
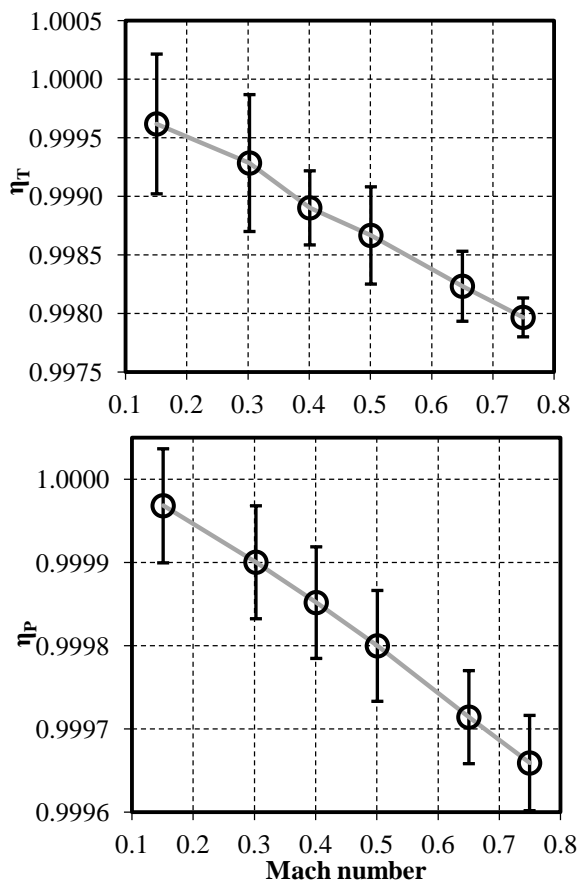

Figure 13: typical calibration curves obtained through the final calibration setup.

The global measurement chain is reported in Figure 14 for the sake of completeness. The nozzle total temperature is acquired by means of four calibrated resistance thermometers. The latter are connected to four Seneca K109pt bridges which provide very low current 4-wire measurement capabilities. At the same location in the nozzle, the feedback thermocouple of the controlled heater and the reference thermocouple of the 2-junction arrangement are also placed.

The nozzle total pressure results from the pneumatic average of six different measurement points along the circumference while the probe's

pressure port is acquired by means of a 2.2 [mbar] Validyne differential pressure transducer, referenced to $P_{0,nozzle}$.

The digitalization of the analog signals is performed by a National Instrument acquisition board except for the measurement of the 2-junction configuration voltage potential which is instead carried out by means of an Agilent 3458A precision voltmeter with a resolution of 10 [nV]. The synchronization of all the devices and the storage of the data is guaranteed by a LabView routine which is also in charge of operating the 2-axis traversing system of the facility.

In the last configuration, the settling time prior to the start of the measurement campaign was reduced to about 7 minutes.
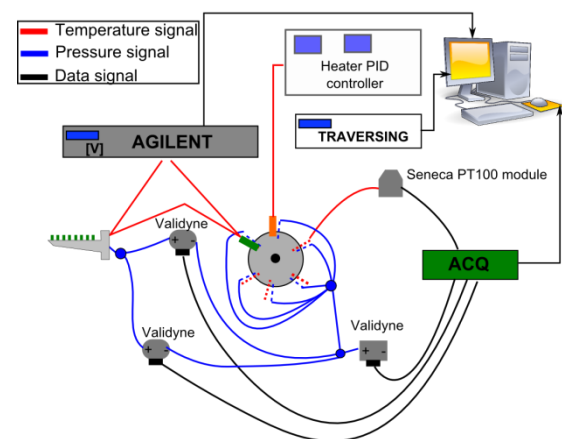

Figure 14: sketch of connections of the final calibration setup and full measurement chain.

UNCERTAINTY ANALYSIS

The uncertainty bars shown in Figure 13 are referred to the 95% confidence interval and they have been computed by means of a type B evaluation [2]. At this extent, care was taken in selecting the most complete set of uncertainty sources that could play a role in its determination.

Taking as an example the resistance thermometers acquiring the nozzle total temperature, one can take into account five main uncertainty contributions:

1. The sensor.
2. The 4-wire measurement bridge electronics.
3. The acquisition board.
4. The stability of the medium (nozzle flow).
5. The network stability.

The sensor's uncertainty results from the propagation of the uncertainty due to the static calibration, to the drift of the static calibration with time, to the interpolation of the static calibration points and to the auto-heating of the platinum resistance.

Stuttgart, Germany
1 - 2 September 2016

The static calibration related uncertainty share can then be broke out in five items:

1. The uncertainty of the reference thermometer (national standards).
2. The stability of the calibration medium.
3. The homogeneity of the calibration medium
4. The acquisition system related uncertainty
5. The network stability

Generally speaking, for every measurement type involved in the frame of a probe calibration, the biggest uncertainty share was always found to be related to the reference device used for the static calibration of the sensors. As an example, the adoption of a calibrated precision thermometer (Isotech TTI-10) as the static calibration reference for the $T_{0,nozzle}$ sensors, allowed to reduce the global uncertainty value of about 20%. In the optic of providing as reliable as possible probes calibrations, than it does make sense to invest in certified reference equipment.

The uncertainty budget related to the electronics appears instead to be rather small. Nevertheless, the global uncertainty of this type of components strongly depends on the last performed self-calibration. The latter feature is present on each type of electronics for laboratory applications and it automatically accounts for the self-heating of the equipment. According to the Agilent 3458A voltmeter specifications, performing a self-calibration for every degree of variation of the ambient temperature allows to reduce this uncertainty item of 80%.

CONCLUSIONS

The development of a highly reliable calibration procedure for total temperature probes was described in the present paper. A step-by-step approach was adopted in order to progressively describe the evolution of the experimental facility and of the measurement chain as a consequence of the analysis of the experimental results.

A lack of accuracy of the measurement chain was identified as the cause to the poor physical meaning of the results obtained by the first experimental campaign. In order to improve the quality of the measurements, a deep analysis of the laws of thermoelectricity was carried out which suggested the adoption of a 2-junctions arrangement for the acquisition of the temperature difference between the nozzle and the probe.

After the implementation of this solution, data acquired a physical dependency with respect to the Mach number even though showing an important scatter and recovery factor values higher than unity at low speeds. The study of the time series of the nozzle total temperature and of the recovery factor in steady blow-down conditions highlighted the presence of a strong conduction effect.

In the final configuration of the experimental setup, an in-line PID controlled heater was mounted upstream the calibration nozzle, providing the nozzle total inlet temperature to be kept at room's conditions (adiabatic calibration). Such modification to the experimental setup drastically improved the quality of the results: the wavy evolution of the measured calibration curved was strongly reduced while the measurement of recovery factor values higher than one was completely avoided.

In the end, for the sake of completeness, the global experimental setup and the whole measurement chain were described while the uncertainty computation methodology was briefly outlined.

ACKNOWLEDGMENTS

REFERENCES

[1] A. Lahalle, *"Experimentally and numerically driven optimization of high performance instrumentation for engine testing"*, Symposium of VKI's doctoral candidate research, March 1-3, 2016, von Karman Institute for Fluid Dynamic.

[2] Bureau International des Poids et Mesures, Commission électrotechnique internationale, and Organisation internationale de normalization, "*Guide to the Expression of Uncertainty in Measurement*". International Organization for Standardization, 1995.